SIN-CHN SCIENTIFIC PRESS PTE.LTD.

Molecular & Cellular Biomechanics 2025, 22(5), 1720.
https://doi.org/10.62617/mcb1720

Article

Integrated biomechanical-thermomechanical approach for hydration heat management in hollow concrete piers: Balancing structural integrity and construction ergonomics

Xiaoyi Hu

School of Urban Construction Engineering, Chongqing Technology and Business Institute, Chongqing 400085, China; hxy@cqtbi.edu.cn

CITATION

Hu X. Integrated biomechanical-thermomechanical approach for hydration heat management in hollow concrete piers: Balancing structural integrity and construction ergonomics. Molecular & Cellular Biomechanics. 2025; 22(5): 1720. https://doi.org/10.62617/mcb1720

ARTICLE INFO

Received: 27 February 2025
Accepted: 21 March 2025
Available online: 27 March 2025

Abstract: This study investigates temperature field variations and associated risks in tall hollow concrete bridge piers caused by cement hydration heat during construction. Integrating field measurements and numerical simulations, we analyzed the dynamic evolution of internal temperature distribution and its structural implications. Field experiments involved continuous temperature monitoring using high-precision sensors embedded in critical zones (core, surface, and varying depths) of a representative pier. Concurrently, a 3D finite element model was developed in ANSYS, incorporating nonlinear thermal properties, the Priestley temperature-dependent hydration model, and realistic boundary conditions. Transient thermal analysis simulated hydration-induced temperature evolution, validated against experimental data. Results revealed significant temperature gradients, with core temperatures rising rapidly due to restricted heat dissipation in large-volume piers. Hydration heat peaked at approximately 70% of maximum temperature within 28 h post-pouring, reaching full intensity at 50 h. Key influencing factors included concrete mix design, cement type, environmental conditions, and cross-sectional dimensions. Post-formwork removal, surface cracking risks escalated due to abrupt temperature differentials, inducing tensile stresses exceeding early-age concrete strength. Mitigation strategies emphasized optimized formwork removal timing, low-heat cement blends (e.g., incorporating fly ash or slag), and enhanced curing techniques (moisture retention, insulation) to regulate thermal gradients. Furthermore, the study highlighted occupational health risks from concentrated heat release, proposing measures such as adjusted work schedules, cooling systems, and protective equipment to safeguard workers. These findings provide actionable insights for balancing structural integrity, construction efficiency, and labor safety in large-scale concrete infrastructure projects. The environmental chamber testing results showed that in a hot environment, the mean skin temperature (35.8 ℃ vs. 36.59 ℃), heart rate (110 beats/min vs. 116 beats/min) and core temperature of the subjects with NCV were significantly lower than those with the control (without NCV). The intelligent monitoring system equipped with sensors has an early warning response time of one minute and a false alarm rate of less than 1%.

Keywords: hydration heat management; thermomechanical analysis; hollow concrete piers; construction ergonomics; biomechanics

1. Introduction

The escalating dimensions of bridge structures have led to a progressive increase in the height and thickness of bridge piers. While existing literature acknowledges the significance of hydration heat in mass concrete structures, research specifically addressing the challenges posed by tall, thick, and hollow concrete bridge piers remains notably limited. Specifically, a comprehensive

understanding of the associated health risks for construction workers and the intricate multi-field coupling effects (e.g., the interplay between thermal stresses, cracking, and environmental factors) in these large-scale structures is still lacking. During the concrete hardening process, the exothermic chemical reaction between cement and water generates hydration heat, causing a temperature rise within the concrete matrix, potentially exceeding 70 ℃ [1]. Conventionally sized concrete members, owing to their efficient heat dissipation, typically exhibit minimal internal-external temperature differentials and are less prone to severe hydration cracking. Conversely, mass concrete structures manifest pronounced hydration characteristics. While the surface heat dissipates relatively rapidly, the heat accumulated within the interior is impeded from timely dissipation, resulting in a significant temperature gradient characterized by elevated internal temperatures and comparatively lower surface temperatures. This non-uniform thermal deformation, coupled with substantial thermal stresses, can induce cracking, particularly exacerbated in larger concrete volumes where temperature differentials and corresponding stresses are amplified [2]. Should these thermal stresses surpass the tensile strength of the concrete, surface cracking may ensue, thereby posing a potential threat to the structural integrity and serviceability [3].

Previous studies have primarily focused on the thermal behavior and cracking mechanisms in conventionally sized or solid mass concrete members. However, the unique geometric characteristics of tall, thick, and hollow bridge piers introduce new complexities in heat dissipation and stress distribution, potentially leading to different patterns of cracking and more pronounced health risks due to prolonged exposure in confined spaces. For instance, the hollow core may impede heat dissipation in certain areas while concentrating it in others, a phenomenon not extensively explored in existing literature. Furthermore, the impact of these specific structural dimensions on the occupational health of workers involved in the construction process, particularly concerning prolonged exposure to elevated temperatures and humidity within the pier, has received limited attention. This study aims to address these critical gaps in the current understanding.

Concurrently, the substantial heat generated by hydration, if not adequately dissipated, presents multifaceted hazards to human health. These encompass a range of heat-related illnesses, including heatstroke, heat exhaustion, and heat cramps, alongside decrements in physiological function such as mental fatigue, diminished work efficiency, and impaired fine motor skills [4]. Furthermore, the combination of high-temperature and humidity environments, compounded by the specific conditions prevalent on construction sites (physical exertion, direct solar radiation, and the use of protective gear), can impede the human body’s thermoregulatory mechanisms, thereby exacerbating these occupational health risks [5].

This research focuses on the temperature field variations and associated engineering risks arising from cement hydration heat during the construction of tall hollow concrete bridge piers. To precisely ascertain the dynamic evolution of the temperature field within these piers and to gain a deeper understanding of the impact of hydration heat on structural safety, we innovatively integrated in-situ measurements with numerical simulations. For the field measurement component, a representative tall hollow concrete bridge pier was selected as the subject of

investigation. High-precision temperature sensors were strategically embedded at critical locations within the pier to enable continuous, real-time monitoring of temperature throughout the concrete casting process and the subsequent hardening phase. The sensor placement encompassed the core region, surface, and varying depths of the pier, aiming to comprehensively capture the nuanced details of the internal temperature distribution.

Meanwhile, to facilitate a more in-depth analysis of the complex temperature field distribution characteristics within the pier under the influence of hydration heat and to provide a theoretical basis for engineering practice, a refined three-dimensional finite element model was developed using ANSYS software. In model construction, meticulous consideration was given to the non-linear thermal properties of the concrete material, the hydration heat generation model, and the actual geometric dimensions and boundary conditions of the pier. A transient thermal analysis was performed to simulate the temperature field evolution process within the pier under hydration heat. The simulation results were then compared and validated against the in-situ measurement data to ensure the accuracy and reliability of the numerical model.

To address the aforementioned limitations in existing research, this study adopts a comprehensive approach based on a three-module framework: experimental investigation, numerical simulation, and the development of health countermeasures. The experimental module will focus on quantifying the hydration heat characteristics and temperature distribution within representative concrete elements that mimic the dimensions of tall, thick, and hollow bridge piers. Subsequently, the numerical simulation module will utilize the experimentally validated data to analyze the multi-field coupling effects, specifically focusing on the evolution of thermal stresses and the prediction of potential cracking risks under various environmental conditions. Finally, the health countermeasures module will propose practical strategies and recommendations to mitigate the identified occupational health hazards associated with hydration heat during the construction of such large-scale bridge piers. The subsequent sections of this paper are structured according to this three-module framework, providing a systematic investigation into the hydration heat challenges in tall, thick, and hollow concrete bridge piers.

2. Materials and methods

2.1. Experimental materials

In this study, P·O42.5R cement, characterized by a specific surface area of 3800 cm^2/g and a loss on ignition of 1.4%, was employed with tap water. The concrete mixture was designed to meet a strength grade of C40. Each cubic specimen was prepared using a mix composition of 322 kg of cement, 750 kg of sand, 1075 kg of aggregate, 105 kg of fly ash, 3.9 kg of water-reducing admixture, and 160 kg of water. Steel formwork was used for casting. The structural parameters and load distribution of the high-pier bridge are detailed in **Figure 1**.

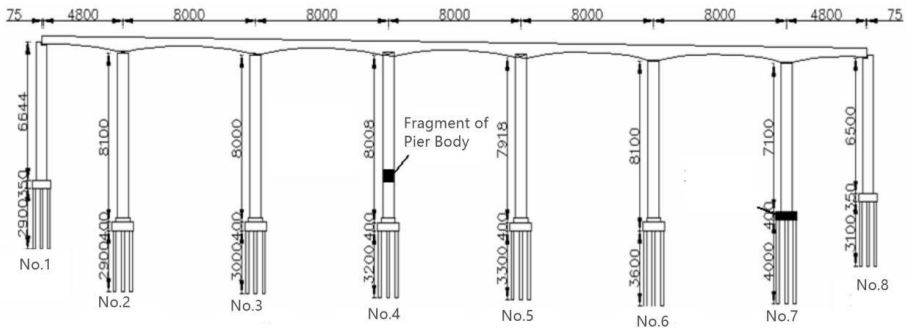

Figure 1. High pier bridge.

The arrangement of temperature monitoring points was strategically planned to capture the thermal behavior of the concrete block comprehensively, including the internal-external temperature gradient, cooling rate, and ambient temperature. Given the symmetrical geometry of the pier segment, a reduced number of sensors were deemed sufficient to representatively monitor the thermal profile. Consequently, ten temperature measurement points were installed (**Figure 2**).

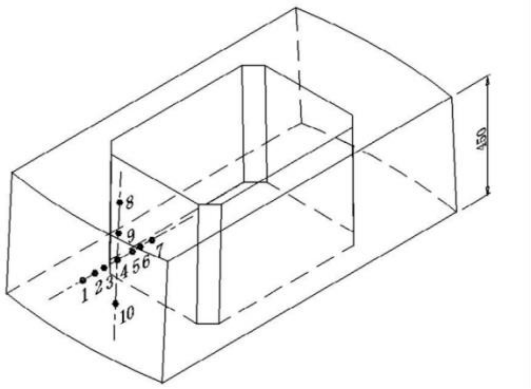

Figure 2. Temperature detection point.

Research manuscripts reporting large datasets that are deposited in a publicly available database should specify where the data have been deposited and provide the relevant accession numbers. If the accession numbers have not yet been obtained at the time of submission, please state that they will be provided during review. They must be provided prior to publication (**Figure 3**).

Figure 3. Temperature sensor.

2.2. Experimental method

Temperature values were recorded at each measurement point for a duration of 450 h after the commencement of concrete pouring in pier segment #2. Due to the rapid fluctuations in hydration heat temperature during the initial concrete pouring phase, the data acquisition interval was set to 2 h. The temperature monitoring system employs AD592 integrated temperature sensors. These sensors offer high measurement accuracy, covering a range from −25 to 105 °C with an error margin of less than ± 0.1 °C. Additionally, each sensor is equipped with a unique ID number, which simplifies data acquisition and recording. The temperature readings are obtained using an LTM8261 handheld multi-point temperature tester. This battery-powered instrument allows for sensor testing and encoding operations independent of a computer. Subsequently, as the rate of temperature change due to hydration heat slowed, the acquisition interval was adjusted to a range of 4 to 10 h. Measurement point 1 was positioned 5 cm from the outer surface of the segment, point 2 at 65 cm, point 3 at 105 cm from the outer surface. Point 4 was located at the central point of the segment, point 5 at 95 cm from the inner surface, point 6 at 60 cm from the inner surface, and point 7 at 5 cm from the inner surface of the segment.

3. Experimental results and analysis

Temperature measurements were conducted on marked points in concrete hollow piers, classified into two categories: outer surface versus central point and inner surface versus central point, to investigate temperature variations in the outer and inner parts of the same cross-section.

3.1. The temperature variation curve from the outer surface to the center point of concrete hollow piers

The hydration temperature curves from the outer surface to the central point of the hollow concrete pier are depicted in **Figure 4**. As illustrated, the hydration temperature exhibited a rapid increase within the initial 28 h post-casting. Notably, the temperature at the central point reached 85% of its maximum temperature rise, and by 50 h, the peak temperature reached 71.3 °C. Subsequently, a gradual temperature decline was observed. Beyond 75 h, a more pronounced temperature decrease occurred. This accelerated cooling is attributed to the removal of formwork at the construction site, which exposed the concrete surface directly to the ambient air. The relatively low environmental temperature and the resultant significant temperature differential facilitated rapid heat dissipation. Measurement point 1, being in close proximity to the outer surface, was significantly influenced by atmospheric temperature fluctuations, exhibiting frequent temperature variations. The temperature difference between the outer surface and the central point initially increased and then decreased, reaching a maximum value of 38.5 degrees Celsius at 115 h, despite measurement point 1 being only 100 cm from the central point.

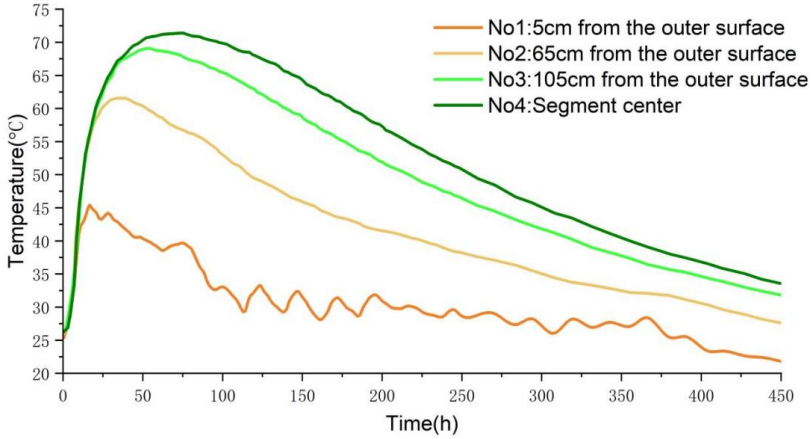

Figure 4. Temperature variation curve from outer surface to center point.

3.2. The temperature variation curve from inner surface to the center point of concrete hollow piers

The hydration temperature curves from the inner surface to the central point of the hollow concrete pier are illustrated in **Figure 5**. The results indicate that within 30 h post-casting, the hydration temperature increased sharply, accounting for approximately 80% of the maximum temperature rise. The peak temperature (68.2 °C) was attained at 60 h post-casting. At 75 h, a rapid decrease in temperature was also observed at the inner surface, again attributed to the removal of formwork, which facilitated extensive heat exchange between the inner surface and the ambient air. As evident from the aforementioned curves, both the concrete surface and the center reached their respective peak temperatures concurrently. However, owing to the low thermal conductivity of concrete, heat dissipation becomes increasingly challenging with distance from the pier surface. Consequently, heat accumulates in the pier center for an extended duration, sustaining a relatively high central temperature [6].

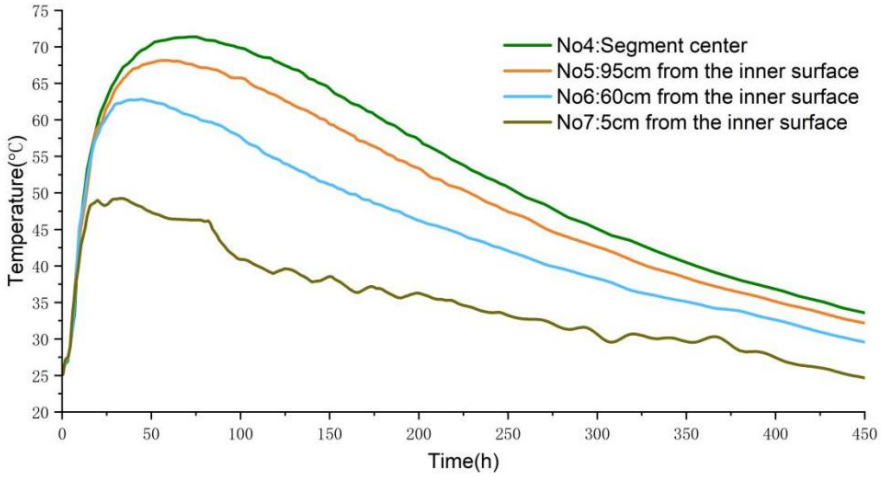

Figure 5. Temperature variation curve from inner surface to center point.

3.3. Cross-sectional variation in concrete hydration heat with depth

As the distance of measurement points from the inner and outer surfaces of the segment increases, the hydration heat temperature of the concrete also rises, with the temperature at the central point being higher than at other measurement locations. Concurrently, the time to reach the peak temperature is also delayed. This phenomenon is attributable to the relatively low thermal conductivity of concrete; as the distance from the inner and outer surfaces of the pier segment increases, heat dissipation becomes more challenging, effectively providing a degree of thermal insulation. Conversely, the temperature at measurement points located 5 cm from the inner and outer surfaces exhibits significant fluctuations. This is because steel formwork, characterized by its higher thermal conductivity, does not provide thermal insulation. Consequently, these measurement points undergo periodic temperature fluctuations in response to ambient air temperature variations both inside and outside the pier segment.

Figures 4 and **5** illustrate the hydration temperature variation curves for surface, interior, and central points. As depicted, temperature fluctuations at the central and surface points are not consistently synchronized. Consequently, the maximum temperature difference between these locations is not merely a simple subtraction of their peak temperatures; rather, the temperature differential increases with time. This phenomenon primarily arises from the inherent low thermal conductivity of concrete, which impedes efficient internal heat dissipation. Given the substantial distance of the pier center from the surface, a significant proportion of the generated heat accumulates internally and dissipates slowly. This results in a gradual and protracted temperature decline at the central point.

Due to the significant influence of external temperature, the surface dissipates heat more rapidly. Consequently, the temperature differential between the interior and exterior increases with time. Even prior to formwork removal, a substantial temperature difference existed between the central and surface points at 240 h post-casting. Upon formwork removal, the surface temperature decreased sharply due to the lower ambient temperature, whereas the central temperature exhibited minimal change owing to the thick cross-section and poor thermal conductivity of the concrete. This resulted in a further increase and a pronounced jump in the interior-exterior temperature differential. As the pouring temperature of mass concrete elevates, both the cooling temperature difference and the temperature difference between the concrete interior and exterior are amplified. This escalation leads to a linear increase in the first principal stress within the structure [7].

Based on the correlation between measurement point temperatures and their distance to the surface, the distribution pattern follows a quadratic polynomial form. Based on this distribution pattern, a temperature value expression for any distance from the surface within the cross-section was formulated as:

$$T_y = T_b - \frac{4y^2}{d^2}(T_z - T_b) + \frac{4y}{d}(T_z - T_b) = T_z - \frac{4 \times (0.5d - y)^2}{d^2}(T_z - T_b) \quad (1)$$

T_y: Temperature at any distance y from the surface within the cross-section (°C).

T_b: Surface temperature of the concrete body at the cross-section (°C).
T_z: Center temperature of the concrete body at the cross-section (°C).
y: Distance from any point to the surface within the cross-section (cm).
d: Thickness of the concrete body at the cross-section (cm).

4. Finite element analysis

Given the limited number of on-site temperature measurement points (only seven), a finite element model was subsequently established using ANSYS software to provide a more comprehensive and visually intuitive understanding of the structural hydration heat distribution. To this end, the aforementioned three-dimensional heat transfer equation was employed, incorporating prevailing site-specific physical conditions, to simulate the hydration heat generation within the structural concrete throughout the entire construction phase.

4.1. Ansys finite element simulation

In this model, the thermal analysis element SOLID70, commonly used in ANSYS for temperature field numerical analysis, was adopted. This element is a three-dimensional (3-D) element with heat conduction capabilities, comprising eight nodes. The degrees of freedom for this element are temperature, and it is classified as a hexahedral element, with each node possessing a single temperature degree of freedom. Based on the geometric dimensions provided in **Figure 2**, a numerical model was established. The model was discretized using a mesh with a minimum element size of 0.2 m. The initial ambient temperature was set to 22 °C. The convective heat transfer coefficient for the concrete surface exposed to outdoor air was defined as 12.5 W/m^2·°C, while the convective heat transfer coefficient for the interior cavity surface in contact with air was set to 9.72 W/m^2·°C. The hydration heat of the concrete was implemented according to Equation (4), with the parameters Q_0 = 340 kJ/kg, a = 0.60, and b = 0.56. Due to the structural symmetry, a quarter section of the structure was adopted for three-dimensional (3D) modeling and meshing. The ANSYS finite element model is illustrated in **Figure 6**.

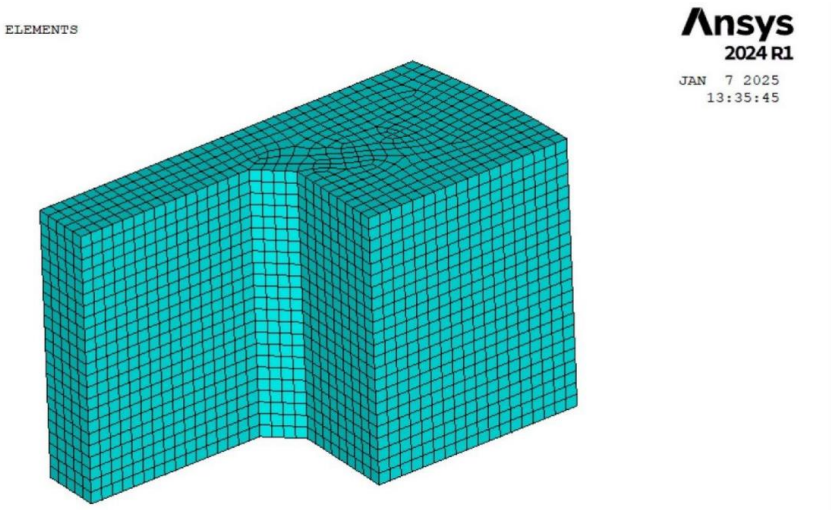

Figure 6. 3D structural mesh model.

In accordance with the principles of finite element analysis, concrete is discretized into numerous elements. Based on the principles of heat conduction and the law of conservation of energy, specifically, the heat absorbed by temperature rise must be equivalent to the sum of the net heat input from the surroundings and the internal heat of hydration. Therefore, the governing differential equation for three-dimensional heat conduction can be formulated as:

$$\rho C \frac{\partial T}{\partial \tau} = \lambda \left(\frac{\partial^2 T}{\partial x^2} + \frac{\partial^2 T}{\partial y^2} + \frac{\partial^2 T}{\partial z^2} \right) + \rho C \frac{\partial \theta}{\partial \tau} \tag{2}$$

where τ denotes time (in hours, h); Crepresents specific heat capacity [in kilojoules per kilogram per degree Celsius, kJ/(kg·°C)]; T signifies temperature (°C); θ is the adiabatic temperature rise of concrete (°C); and ρ is the mass density of concrete (in kilograms per cubic meter, kg/m^3):

In the context of this project, the heat of hydration of concrete can be characterized using the following two equations:

$$\theta(\tau) = Q(\tau)(W + kF)/cp \tag{3}$$

$$Q(\tau) = Q_0\left(1 - \exp\left(-a\tau^b\right)\right) \tag{4}$$

W: Cement dosage (amount of cement used).

F: Dosage of supplementary cementitious materials (SCMs) (amount of SCMs used).

k: Reduction coefficient (for fly ash, k = 0.25).

$Q(\tau)$: Cumulative heat of hydration at age, τ: age.

Q_0: Total heat of hydration of cement (kJ/kg); coefficients a and b are constants.

4.2. Finite element analysis of hydration heat temperature field in hollow concrete piers

In this study, ANSYS finite element analysis was employed to simulate the hydration heat temperature distribution, taking into account site-specific construction conditions. The numerical model incorporated factors such as layered concrete pouring, layer thickness, hydration heat temperature rise variation, creep, material zoning, pouring temperature, and convective boundary conditions. Following the actual experimental sequence, load step sizes were judiciously selected to account for the influence of construction pauses. The resulting hydration heat temperature distributions at 75 h, 200 h, and 400 h are presented in the following (**Figures 7–9**).

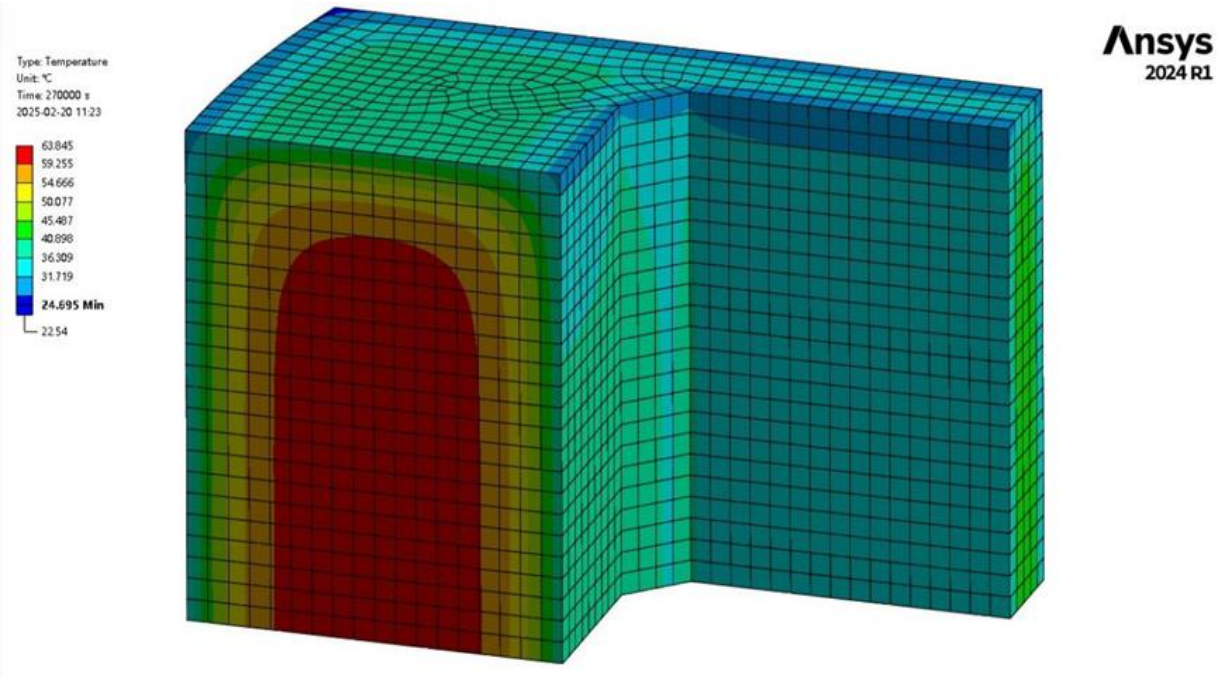

Figure 7. Hydration heat distribution at 75 h.

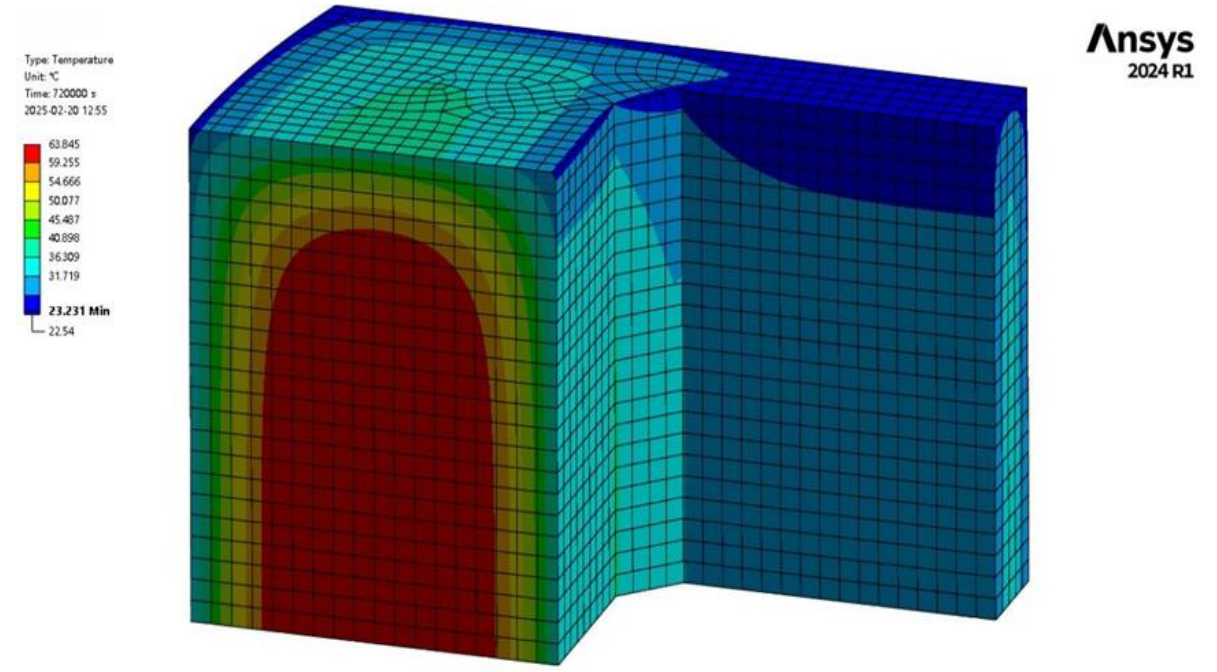

Figure 8. Hydration heat distribution at 200 h.

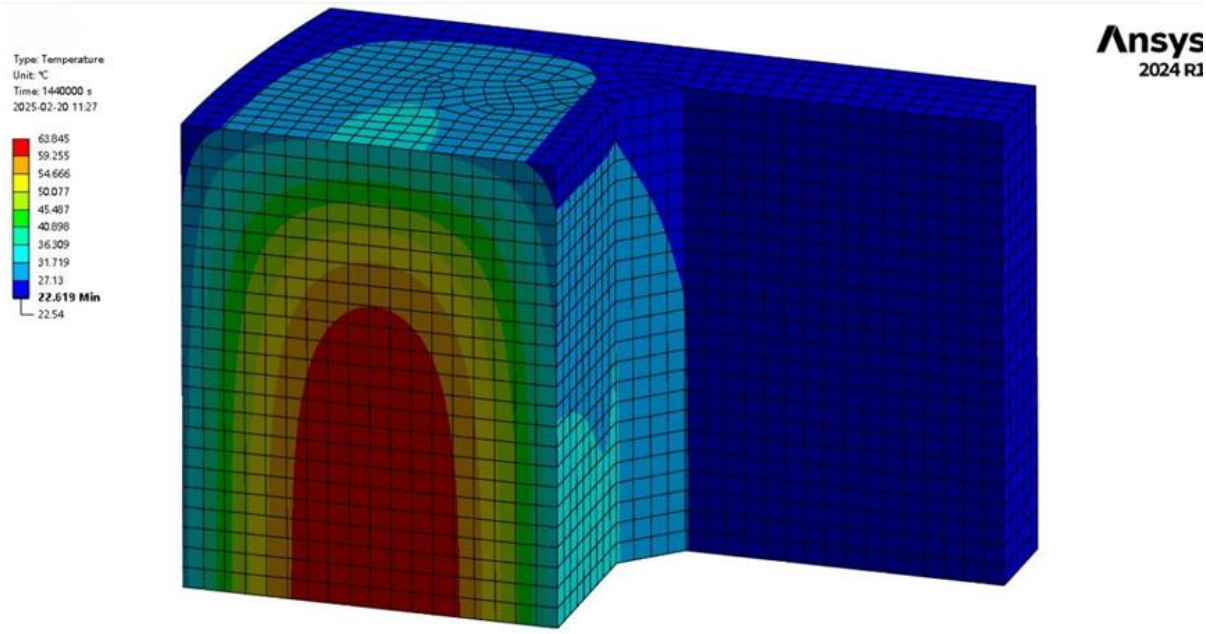

Figure 9. Hydration heat distribution at 400 h.

The aforementioned three figures demonstrate that the temperature variations along the cross-section exhibit similar trends across different time points. As time progresses, the temperature at all measurement points, both internal and external, increases due to the heat released from cement hydration. The hydration heat temperature peaks at approximately 70 h, the simulation analysis yielded a result of 63.8 degrees, while the measured value was approximately 67.8 degrees, indicating a close agreement between the numerical and experimental results. Subsequently, the temperature gradually decreases, which can be attributed to the formwork removal around that time when the external temperature is significantly lower than the surface temperature. Under these circumstances, the surface releases heat to the surroundings, resulting in a noticeable temperature reduction. The temperature variation curves for the central and surface points are generally consistent; however, the peak temperature at the concrete surface is evidently lower than the peak temperature observed in the interior.

5. Biomechanical effects of high heat and countermeasures

5.1. Impact of concrete hydration heat on construction workers

Based on the aforementioned temperature field analysis, the subsequent section will explore its impact on human health. During the construction of tall bridge piers, the concentrated release of hydration heat from mass concrete can elevate surface temperatures to 40 °C within a single day, posing a significant challenge to the health and safety of construction workers.

High-temperature work environments can induce heat stress responses in the human body. When core body temperature exceeds 38 °C, the human thermoregulatory system faces significant challenges [8]. Research indicates that in a 35 °C environment, construction workers engaged in continuous work for 2 h experience a 15%–20% increase in cardiac output and a sweat loss rate reaching 1.5

L/h. The cumulative effect of such physiological strain may trigger life-threatening occupational diseases such as heatstroke and rhabdomyolysis.

Empirical evidence demonstrates that for every 1-degree Celsius increment in ambient temperature, there is an approximate 2% reduction in manufacturing productivity at the factory scale [9]. This phenomenon is particularly salient during periods of extreme heat and in manufacturing environments characterized by high worker value contribution. Elevated thermal conditions significantly impair cognitive functions related to labor, most notably impacting volitional work engagement, as evidenced by a reduction in both the median and amplitude of work willingness under heat stress. Furthermore, research findings indicate an inverse relationship between indoor temperature and response time, positing a potential decrement in decision-making efficacy [10]. Heat-induced stress precipitates confusion, heightened irritability, and emotional distress amongst employees, which may culminate in diminished attentiveness to tasks or neglect of established safety procedures [11]. Consequently, the elevated thermoregulatory burden coupled with perceived exertion amplifies the probability of personnel resorting to unsafe operational behaviors or contravening safety regulations under conditions of thermal overload [12].

Moreover, prolonged exposure to high ambient temperatures poses a significant detriment to workers' cardiovascular health, with Nepalese migrant laborers in Qatar being particularly vulnerable [13]. Epidemiological investigations have revealed a robust correlation between elevated Wet Bulb Globe Temperature (WBGT) and a heightened incidence of cardiovascular disease (CVD) mortality, noting that a substantial proportion (58%) of CVD-related deaths occur during periods of elevated thermal intensity. A considerable number of these fatalities are ascribed to heatstroke, implying that acute heat stress has the propensity to aggravate underlying cardiovascular vulnerabilities. Occupational heat exposure precipitates increased cardiovascular burden as a consequence of elevated core body temperature, a phenomenon that is particularly pronounced amongst elderly workers exhibiting compromised thermoregulation. Concomitantly, diminished sudorific responses and impaired thermolytic mechanisms exacerbate this physiological stress, thereby escalating the susceptibility to heat-related morbidities.

5.2. Individual protective equipment and countermeasures for high-temperature and extreme heat

Modern personal protective technologies for high-temperature operations have evolved into a multimodal collaborative protection system. For instance, Guo et al. developed a newly designed cooling vest for construction workers, which utilizes phase change materials (PCM) to combat heat stress. The environmental chamber testing results showed that in a hot environment, the mean skin temperature (35.8 ℃ vs. 36.59 ℃), heart rate (110 beats/min vs. 116 beats/min) and core temperature of the subjects with NCV were significantly lower than those with the control (without NCV) [14]. Del Ferraro and associates have engineered a ventilated jacket as a form of personal cooling garment for construction personnel, with the explicit objective of augmenting evaporative thermal dissipation and diminishing physiological heat

strain (**Figure 10**). Their experimental investigations revealed that escalating fan velocities engender a marked augmentation of evaporative heat flux, particularly within the thoracic region, demonstrating amelioration exceeding 100% upon fan actuation [15]. Furthermore, when integrated with conventional work ensembles, the jacket exhibits a notable reduction in total evaporative impedance, thereby underscoring its prospective utility as a viable cooling modality for outdoor occupational settings, and for the efficacious attenuation of core body temperature escalation.

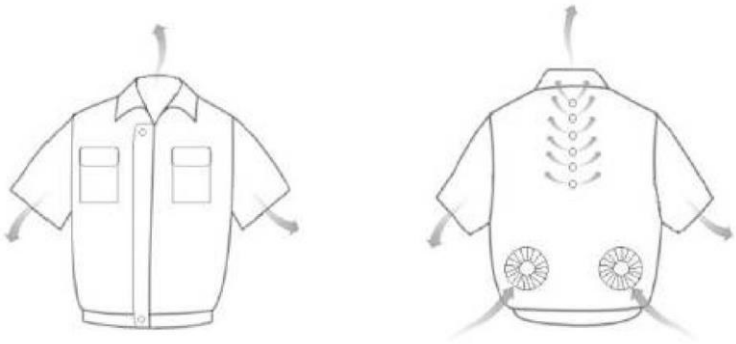

Figure 10. The ventilation jacket with six circular openings and two fans placed in the back site.

A sophisticated Internet of Things (IoT)-enabled platform for physiological data surveillance has been developed, specifically tailored for construction personnel laboring in thermally challenging environments [16]. This system leverages wearable smart wrist-worn devices, incorporating an array of sensors (photoplethysmography (PPG), accelerometer, and cutaneous temperature transducers) to facilitate comprehensive individual health risk evaluation. The intelligent monitoring system equipped with sensors has an early warning response time of one minute and a false alarm rate of less than 1%. It features an integrated holistic thermal assessment module, which dynamically governs work-rest cycles based on established heat comfort metrics. The platform architecture facilitates remote real-time monitoring of worker physiological status and geolocation by authorized supervisors, thereby ensuring prompt medical or safety interventions as warranted. Furthermore, Li et al. implemented infrared thermography sensors embedded within smart helmet assemblies for non-invasive body temperature monitoring of construction laborers, presenting an economically viable and robust methodology for continuous temperature surveillance [17]. Their investigation culminated in the development of a Partial Least Squares Regression—Backpropagation Neural Network (PLS-BPNN) error rectification algorithm, designed to optimize measurement accuracy, demonstrably minimizing the relative mean deviation and enhancing the fidelity of thermal measurements acquired in construction settings.

In Japan, a dedicated Construction Worker Heatstroke Prevention (CWHP) system has been implemented, designed to forecast thermal conditions and core body temperature as a means of evaluating heatstroke susceptibility. The CWHP system leverages environmental sensor networks and meteorological data from the Japan Meteorological Agency to apprise construction supervisors of impending heatstroke

risks, thereby facilitating the proactive implementation of optimized work schedules and safety protocols [18]. Kakamu et al. further elaborated on the application of wearable sensor technologies, exemplified by the LW-360HR device, which provides tri-minute monitoring of key physiological parameters, including heart rate and cutaneous temperature. Such sensor modalities are instrumental for the dynamic assessment of physiological responses to thermal stress, enabling continuous health surveillance and the mitigation of heat-related morbidities amongst construction laborers in thermally challenging outdoor settings. The trajectory of personal protective equipment (PPE) for high-temperature and high-heat occupational environments is demonstrably shifting towards intelligent and adaptive functionalities.

Furthermore, the strategic implementation of nutritional adjuncts may confer protective benefits to workers [19]. Betaine supplementation has been shown to potentiate thermotolerance in humans, exhibiting particular salience for occupational groups subjected to elevated thermal loads, such as construction laborers. The functional mechanism of betaine is analogous to that of molecular chaperones, serving to stabilize protein tertiary structure and attenuate oxidative injury during episodes of heat stress. The effective management of construction workforces in hyperthermic settings necessitates a systematic, multi-faceted paradigm for thermal stress mitigation [20]. Core components of this paradigm encompass the establishment of environmental heat exposure control measures predicated upon actionable thresholds, the enforcement of continuous work duration protocols, the provision of compulsory rest intervals, and the empowerment of personnel to engage in self-regulated work pacing. Moreover, comprehensive heat-related illness prophylaxis initiatives are integral to effective workforce management, including rigorous educational modules on heat stress pathophysiology and symptomatic identification. Employers bear the responsibility to ensure the provision of adequate resources, such as hydration, shaded refuge, and scheduled respite, to ameliorate heat-associated occupational hazards [21]. Corporate entities are thus urged to formulate explicit heat illness management protocols and to rigorously disseminate relevant information to personnel, with the overarching aim of minimizing the prevalence of heat-related morbidities within outdoor occupational environments.

5.3. Behavioral interventions for heat stress management among construction workers

In high-temperature work environments, construction workers are compelled to proactively implement a range of behavioral interventions. This proactive approach is essential to construct a robust multi-layered self-protection system, designed to mitigate the significant health risks associated with intense heat exposure. Firstly, the implementation of graded heat acclimatization training is paramount. This training regimen should involve a daily incremental increase of 20% in work duration, sustained over a period of 7 to 14 days. This gradual exposure is crucial for enhancing physiological heat tolerance thresholds, effectively preparing the body to withstand thermal stress. Furthermore, this acclimatization process is vital in

reducing the risk of electrolyte loss, a common and potentially dangerous consequence of prolonged heat exposure.

Secondly, the scientific and judicious selection of personal protective equipment (PPE) is of utmost importance to extend the effective duration of protection against heat. PPE acts as a crucial barrier, reducing direct heat exposure and mitigating its harmful effects. Concurrently, to ensure continuous monitoring of workers' health status, an autonomous health monitoring mechanism should be meticulously established. This mechanism should leverage wearable devices to track core body temperature in real-time, allowing for immediate detection of hyperthermia or other heat-related physiological changes:

Furthermore, the adoption of a carefully structured “20-minute high-intensity and minute low-intensity” intermittent work pattern is recommended. This specific work cycle can effectively reduce metabolic heat generation during intense labor. By incorporating periods of lower-intensity activity, the body has an opportunity to dissipate heat and prevent excessive internal temperature build-up.

Moreover, to enhance workers’ capacity to respond effectively to heat-related emergencies, it is also necessary to internalize the World Health Organization (WHO) three-stage recognition criteria for heat-related illnesses. This understanding of the progression of heat illnesses is vital for timely intervention. Workers must master essential emergency skills, encompassing rehydration strategies during the compensation stage, axillary cooling techniques during the decompensation stage, and when necessary, the more aggressive intervention of cold water immersion during the organ damage stage. These skills are critical for providing immediate and appropriate first aid, potentially preventing severe health outcomes and ensuring worker safety in demanding high-temperature environments (**Figure 11**).

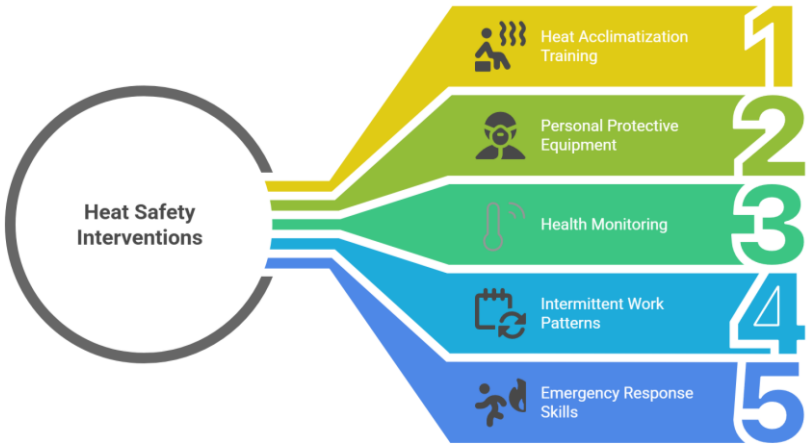

Figure 11. Heat safety interventions.

6. Conclusion

Robust empirical datasets were acquired via the sustained monitoring of the hydration temperature field within hollow concrete bridge pier structures. A finite element numerical model was subsequently developed to analyze the hydration heat generation characteristics of high pier foundations. The temporal temperature

variation patterns identified herein serve as a valuable reference for the constructional execution of analogous engineering projects. The following conclusions were drawn from this investigation:

The issue of hydration heat-induced hazards in massive concrete bridge piers warrants the utmost attention from engineering professionals. Empirical findings can be utilized as preliminary reference data prior to concrete placement, offering valuable insights into the intensity and spatial allocation of thermal control strategies.

Subsequent to the completion of concrete casting in bridge piers, a recession in the thermal gradient between the internal core and external surface is observed within a brief post-formwork removal interval. This temporal phase constitutes a period of heightened susceptibility to surface cracking phenomena in the pier structure. Consequently, the determination of formwork stripping timing should be approached with circumspection, and commensurate interventions should be enacted to mitigate thermal variations, thereby diminishing the probability of superficial fissure formation on the pier exterior.

Elevated ambient temperatures in construction work zones, attributable to hydration heat emanating from voluminous concrete structures, present manifold health hazards to construction personnel. Episodes of acute thermal exposure may precipitate heatstroke and elevate susceptibility to rhabdomyolysis. Effective thermoregulation and risk mitigation can be attained through the provision of phase change material-integrated thermoregulatory apparel to construction workers, in conjunction with the implementation of biometric sensor networks for dual-frequency microwave-based core temperature surveillance. Looking ahead, the evolutionary trajectory of personal protective equipment (PPE) intended for arduous, high-temperature, and high-heat occupational settings is projected to converge towards intelligent and sustainable paradigms.

Funding: This research was funded by the Science and Technology Research Program of Chongqing Municipal Education Commission, grant number KJQN202104012.

Ethical approval: Not applicable.

Conflict of interest: The author declares no conflict of interest.

References

1. Zhou J, Li X, Wang Z, et al. Numerical Analysis of Temperature Stress Generated by Hydration Heat in Massive Concrete Pier. Periodica Polytechnica Civil Engineering. 2025. doi: 10.3311/ppci.38403
2. Wang S, Xu J, Zhong R. Temperature control technology on construction of large volume concrete. Advances in Engineering Technology Research. 2024; 11(1): 388. doi: 10.56028/aetr.11.1.388.2024
3. Klemczak B, Smolana A. Multi-Step Procedure for Predicting Early-Age Thermal Cracking Risk in Mass Concrete Structures. Materials. 2024; 17(15):3700. https://doi.org/10.3390/ma17153700
4. Savioli G, Zanza C, Longhitano Y, et al. Heat-Related Illness in Emergency and Critical Care: Recommendations for Recognition and Management with Medico-Legal Considerations. Biomedicines. 2022; 10(10): 2542. doi: 10.3390/biomedicines10102542

5. Torbat Esfahani M, Awolusi I, Hatipkarasulu Y. Heat stress prevention in construction: A systematic review and meta-analysis of risk factors and control strategies. International journal of environmental research and public health. 2024; 1(12): 681. doi: 0.3390/ijerph21121681
6. Al-rawi RS, Salih S mahdi. Control o Thermal And Shrinkage Cracking o Mass Concrete in Hot Climate. Journal of Engineering. 2024; 9(02): 195-205. doi: 10.31026/j.eng.2003.02.04
7. Saksala T. Demolition of concrete by thermal shock spallation: a mesoscopic numerical study based on embedded discontinuity finite elements. International Journal of Fracture. 2020; 225(2): 191-217. doi: 10.1007/s10704-020-00474-y
8. Stacey MJ, Delves SK, Britland SE, et al. Copeptin reflects physiological strain during thermal stress. European Journal of Applied Physiology. 2017; 118(1): 75-84. doi: 10.1007/s00421-017-3740-8
9. Sudarshan A, Tewari M. The economic impacts of temperature on industrial productivity: Evidence from Indian manufacturing. Indian Council for Research on International Economic Relations (ICRIER), New Delhi. 2014.
10. Zheng G, Li K, Bu W, et al. The Effects of Indoor High Temperature on Circadian Rhythms of Human Work Efficiency. International Journal of Environmental Research and Public Health. 2019; 16(5): 759. doi: 10.3390/ijerph16050759
11. Dear K. Modelling Productivity Loss from Heat Stress. Atmosphere. 2018; 9(7): 286. doi: 10.3390/atmos9070286
12. Tokizawa K. Heat-induced labor loss and growing global concerns in a warmer world. Industrial health. 2022; 60(6): 499-500. doi: 10.2486/indhealth.60_600
13. Pradhan B, Kjellstrom T, Atar D, et al. Heat Stress Impacts on Cardiac Mortality in Nepali Migrant Workers in Qatar. Cardiology. 2019; 143(1-2): 37-48. doi: 10.1159/000500853
14. Guo Y, Chan AP, Wong FK, et al. Developing a hybrid cooling vest for combating heat stress in the construction industry. Textile Research Journal. 2017; 89(3): 254-269. doi: 10.1177/0040517517743685
15. Del Ferraro S, Falcone T, Morabito M, et al. A potential wearable solution for preventing heat strain in workplaces: The cooling effect and the total evaporative resistance of a ventilation jacket. Environmental Research. 2022; 212: 113475. doi: 10.1016/j.envres.2022.113475
16. Kim JH, Jo BW, Jo JH, et al. Development of an IoT-Based Construction Worker Physiological Data Monitoring Platform at High Temperatures. Sensors. 2020; 20(19): 5682. doi: 10.3390/s20195682
17. Li L, Yu J, Cheng H, et al. A Smart Helmet-Based PLS-BPNN Error Compensation Model for Infrared Body Temperature Measurement of Construction Workers during COVID-19. Mathematics. 2021; 9(21): 2808. doi: 10.3390/math9212808
18. Yabuki N, Onoue T, Fukuda T, et al. A heatstroke prediction and prevention system for outdoor construction workers. Visualization in Engineering. 2013; 1(1). doi: 10.1186/2213-7459-1-11
19. Willingham BD, Ragland TJ, Ormsbee MJ. Betaine Supplementation May Improve Heat Tolerance: Potential Mechanisms in Humans. Nutrients. 2020; 12(10): 2939. doi: 10.3390/nu12102939
20. Baizhan L, Andrew B. Meeting the challenge of climatic heat stress in construction. Industrial health. 2018; 56(4): 275-277. doi: 10.2486/indhealth.56_400
21. Asher M.S TD, McAndrew I. Heat Illness Prevention in the Outdoor Workplace. Health Informatics—An International Journal. 2021; 10(02): 1-4. doi: 10.5121/hiij.2021.10201